ChemComm

Fluoride-free synthesis of high-silica CHA-type aluminosilicates by seed-assisted aging treatment for starting gel

Journal:	*ChemComm*
Manuscript ID	CC-COM-07-2022-004032.R1
Article Type:	Communication

COMMUNICATION

Fluoride-free synthesis of high-silica CHA-type aluminosilicates by seed-assisted aging treatment for starting gel†

Received 00th January 20xx,
Accepted 00th January 20xx

DOI: 10.1039/x0xx00000x

Ryota Osuga,[*a] Mizuho Yabushita,[b] Takeshi Matsumoto,[c] Masato Sawada,[c] Toshiyuki Yokoi,[c] Kiyoshi Kanie,[a,d] and Atsushi Muramatsu[*a,d]

High-silica CHA-type aluminosilicates (Si/Al molar ratio > 100) were synthesized hydrothermally in the absence of fluoride media, where the seed-assisted aging treatment played an important role on the crystallization. These aluminosilicates showed a long catalytic lifetime with high selectivity toward lower olefins in the methanol-to-olefins reaction.

Zeolites, which are porous crystalline materials, have been widely used as solid acid catalysts in the petrochemical field.[1] Their acidity originates from the bridging OH group between Si and Al atoms in their aluminosilicate framework. The demand for 8-ring (8R) zeolites and zeotype materials has been increasing in recent decades because their small pores exhibit unique shape selectivity toward small molecules.[1c] Among them, **CHA**-type zeolites, represented by chabazite, are well-known cage-structured 8R zeolites that have been industrially applied as adsorbents, gas-separators, and catalysts. [1c,2] Chabazite, the type material of **CHA**-type zeolites, was discovered as a naturally occurring aluminosilicate by Dent and Smith in 1958 and is a typical low-silica zeolite (Si/Al molar ratio of 2).[3] In general, zeolite synthesis methods that enable control of the Si/Al ratio are attractive for industrial applications because the Si/Al ratio for zeolites is strongly related to their hydrophilicity, acidity, and hydrothermal stability.[1]

SSZ-13, which is a high-silica **CHA**-type aluminosilicate,[4] has been developed by numerous research groups, and the controllable range of its Si/Al molar ratio has been expanded to *ca.* 100 using organic-structure-directing agents (OSDAs) and seed crystals.[5] SSZ-13 is often used as a catalyst for the methanol-to-olefins (MTO) reaction because it can convert methanol at low temperatures (*ca.* 300 °C) and with high selectivity to ethene and propene as a consequence of its small pores and strong Brønsted acid sites.[6] However, there are some disadvantages to using **CHA**-type aluminosilicates as catalysts for the MTO reaction:[5c,7] 1) a large amount of paraffin is generated at the initial stage, and 2) the catalyst lifetime is short. These drawbacks arise from the excessive progression of consecutive reactions due to the **CHA**-type aluminosilicates' high density of active sites and strong acidity. To address these issues, increasing the Si/Al molar ratio (*i.e.*, decreasing the number of acid sites) is an effective approach that leads to improvements in hydrothermal stability, selectivity toward lower olefins, and catalyst lifetime. However, increasing the Si/Al molar ratio for **CHA**-type zeolites to greater than 100 requires some specific synthesis conditions.[8] Such **CHA**-type zeolites can be synthesized in the presence of fluoride media with an extremely low H_2O/SiO_2 ratio in the starting gel (Table S1, ESI†); however, the use of fluoride species should be avoided because of their adverse environmental effects. Also, the addition of fluoride species promotes crystal growth, resulting in relatively large particles.[9] These large particles retard molecular diffusion and cause excessive progression of consecutive reactions.[10] Recently, Jabri *et al.* reported the synthesis of a high-silica SSZ-13 in the absence of fluoride media using a dry-gel conversion technique, achieving a maximum Si/Al ratio of 182.[8c] In addition, Zhang *et al.* successfully synthesized **CHA**-type aluminoborosilicates using *N*,*N*,*N*-trimethylisobutylammonium hydroxide as an OSDA.[8d] These methods, however, require a complicated multistep preparation that is difficult to conduct industrially. Thus, a novel and easy-to-handle method for synthesizing high-silica **CHA**-type aluminosilicates under fluoride-free and simple crystallization conditions is desired.

The fluoride-free hydrothermal synthesis method used in most previous related studies results in undesirable phases such as **AFI** and **MWW** in addition to high-silica **CHA**-type zeolite.[5b]

The types of silicate species dissolved in the starting gel are generally regarded as the critical factor for controlling the resultant zeolite structure. Besides, the addition of seed crystals into the gel is a well-known effective method of inducing crystallization of the desirable zeolite phase because the seed crystals provide specific building units that lead to the construction of the target zeolite framework.[11] However, the conventional method of synthesizing high-silica **CHA**-type aluminosilicates by adding seed crystals immediately before a hydrothermal treatment cannot provide a starting gel with a sufficient amount of the preferred units for the **CHA** phase. Therefore, in our synthetic strategy developed in the present study, the formation of the preferred building units for the **CHA** phase in the starting gel is induced by an aging treatment of the

[a] *Institute of Multidisciplinary Research for Advanced Materials, Tohoku University, Sendai, 2-1-1 Katahira, Aoba-ku, Miyagi 980-8577, Japan.*
[b] *Department of Applied Chemistry, School of Engineering, Tohoku University, 6-6-07 Aoba, Aramaki, Aoba-ku, Sendai, Miyagi 980-8579, Japan.*
[c] *Institute for Innovative Research, Tokyo Institute of Technology, 4259 Nagatsuta, Midori-ku, Yokohama 226-8503, Japan.*
[d] *International Center for Synchrotron Radiation Innovation Smart, Tohoku University, 2-1-1 Katahira, Aoba-ku, Sendai, Miyagi 980-8577, Japan.*
†Electronic Supplementary Information (ESI) available: Experimental, calculating methods and characterization data. See DOI: 10.1039/x0xx00000x

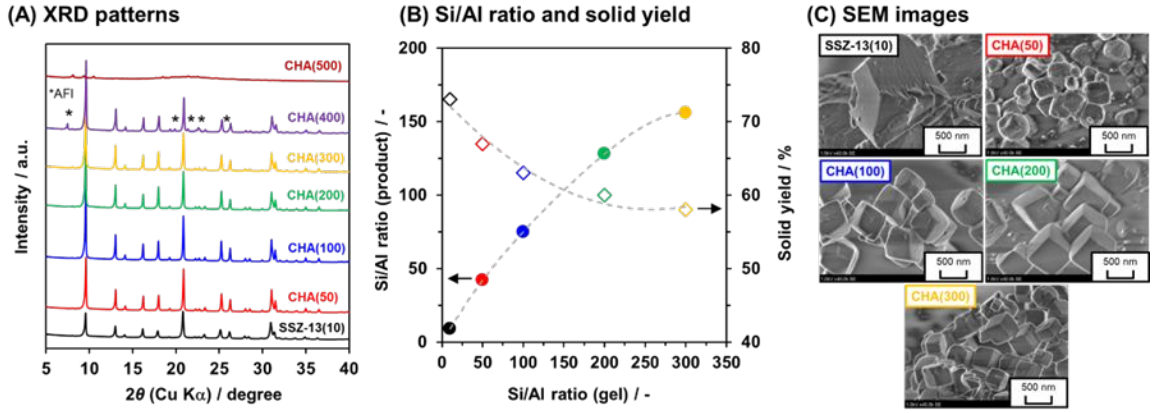

Fig. 1 (A) XRD patterns, (B) Si/Al molar ratio and solid yield, and (C) SEM images of the synthesized **CHA**-type aluminosilicates.

gel containing seed crystals (hereinafter referred to as "seed-assisted aging"), which is a novel approach to crystallizing high-silica **CHA**-type aluminosilicates. In addition, the catalytic performance of the obtained high-silica **CHA**-type aluminosilicate toward the MTO reaction was compared with that of the conventional SSZ-13 zeolite.

Using our aforementioned synthesis strategy, we synthesized high-silica **CHA**-type aluminosilicates with various Si/Al molar ratios via seed-assisted aging in the absence of fluoride media. Prior to the synthesis of the high-silica **CHA**-type aluminosilicates, seed crystals of SSZ-13(10) (where the number in parentheses indicates the Si/Al molar ratio of the starting gel) was prepared via a previously reported method.[12] For the synthesis of the high-silica **CHA**-type aluminosilicates, a seed crystal (2 wt% to SiO_2) was added to starting gels that contained all the raw materials; the gel was then aged at room temperature for 24 h to create preferred building units for the **CHA** phase (*e.g.*, 6-6, 6, 4-2, 4, *d6r*, and *cha*, see Fig. S1, ESI†). The thus-prepared gels were hydrothermally treated at 170 °C for 48 h. The obtained samples are designated as CHA(*X*), where *X* indicates the Si/Al molar ratio in the starting gel. The experimental details are described in the Experimental section (ESI†). To investigate the formation of the preferred units for the **CHA** phase in the starting gel, we used electrospray ionization mass spectroscopy (ESI-MS) to analyze the dissolved aluminosilicate species in the liquid phase of the starting gels (Fig. S2, ESI†). A comparison of the ESI-MS spectra of the gels with and without seed crystals added during the aging treatment reveals that the amount of even-ring species[11b,13] in the gel aged with a seed crystal was greater than that in the gel aged without seed crystals (Table S2, ESI†). These results indicate that the seed-assisted aging treatment could provide preferable building units for the **CHA** phase, the even-ring species, in the starting gel.

Fig. 1(A) shows the XRD patterns of the synthesized H^+-form samples. When the Si/Al molar ratio in the gel was in the range from 50 to 300, the diffraction peaks corresponding to the **CHA**-type structure were observed as a single phase. By contrast, **AFI**-type and amorphous phases were detected in the CHA(400) and CHA(500) samples, respectively. Moreover, the diffraction peaks for the high-silica **CHA**-type aluminosilicates were more intense than those for the SSZ-13(10), suggesting that the synthesized high-silica **CHA**s exhibit better crystallinity than the SSZ-13.

The effect of the seed-assisted aging time was investigated. The XRD patterns of CHA(300) with different aging times are compared in Fig. S3 (ESI†). The single **CHA**-type phase was confirmed in the samples aged for 3 h or longer, whereas a halo due to an amorphous phase and much lower intensity of the diffraction peaks derived from the **CHA** phase were observed in the sample without the seed-assisted aging. In addition, the Si/Al ratio increased with increasing the aging time. These results clearly indicate the positive effect of the seed-assisted aging treatment on the crystallization of high-silica **CHA**-type aluminosilicates. Consistent with these results, Kong *et al.* also reported the importance of the aging time on the crystallization of all-silica **CHA** zeolites with fluoride media.[8e]

The actual Si/Al molar ratios for the synthesized samples, as determined by inductively coupled plasma atomic emission spectroscopy (ICP-AES) measurements, are summarized in Table 1. The highest Si/Al ratio was 156, which was obtained for CHA(300). This Si/Al ratio is the highest ever reported for a **CHA**-type aluminosilicate synthesized under fluoride-free conditions. The Si/Al molar ratios and the solid yields for each sample are plotted in Fig. 1(B), where the Si/Al ratio for the product increased with increasing Si/Al ratio in the starting gel. However, the solid yields decreased with increasing Si/Al ratio in the gel. Given the difference in the Si/Al molar ratio between the starting gel and the product, the decrease in the solid yield might be caused by poor Si incorporation into the framework, which is a common phenomenon observed in the synthesis of **CHA**-type aluminosilicates.[14] An interesting finding was also observed in the particle morphology (Fig. 1(C)). In the general synthesis conditions using fluoride media, the particle size was micrometer order.[9b,15] In contrast to previously reported studies, small cubic particles (*ca.* 500 nm) were observed in the samples synthesized by the seed-assisted aging treatment, suggesting that the presence of seed crystals promoted the nucleation and the absence of fluoride media inhibited unnecessary crystal growth. In addition, compared with the SSZ-13(10), the as-prepared CHA(*X*)s contained a greater amount of OSDAs (Table 1), which is also one of the origins of the high Si/Al ratio.

Table 1 Physicochemical properties of each sample.

Samples	Si/Al[a]	Amount of OSDA[b]		Solid yield	Specific surface area[c]	Micropore volume[d]	Number of acid sites[e]	
	/ -	/ mmol g^{-1}	/ molecules $cage^{-1}$	/ %	/ m^2 g^{-1}	/ cm^3 g^{-1}	/ mmol g^{-1}	/ sites $cage^{-1}$
SSZ-13(10)	9	0.76	0.57	73	751	0.26	0.77	0.57
CHA(50)	42	1.09	0.82	67	885	0.32	0.34	0.23
CHA(100)	75	1.18	0.89	63	881	0.33	0.18	0.13
CHA(200)	128	1.13	0.85	60	868	0.33	0.09	0.07
CHA(300)	156	1.18	0.89	58	878	0.30	0.05	0.03

Determined by [a]ICP-AES, [b]TG-DTA, [c,d]N_2 physisorption, and [e]NH_3-TPD.

The physicochemical properties of the synthesized samples were characterized. N_2 physisorption measurements resulted in **in** typical type-I isotherms for all the samples (Fig. S4, ESI†). The Brunauer–Emmett–Teller (BET) specific surface area and micropore volume of a series of CHA(*X*) were larger than those of SSZ-13(10), which might be attributable to the difference in crystallinity of the samples (Fig. 1). The coordinating structure of Al atoms was investigated by ^{27}Al magic-angle-spinning (MAS) NMR spectroscopy. In the ^{27}Al MAS NMR spectra shown in Fig. S5(A) (ESI†), the peak at 59 ppm, which is assignable to tetrahedrally coordinated Al species (*i.e.*, intra-framework Al species),[16] was observed, along with minor peaks at 0 ppm corresponding to the octahedrally coordinated Al species (*i.e.*, extra-framework Al species).[16] These spectra indicate that Al atoms incorporated into the framework are major species.

The number of acid sites and their strength were examined by temperature-programmed desorption with NH_3 (NH_3-TPD) (Fig. S5(B), ESI†). The peaks observed at approximately 250–550 °C can be assigned to the NH_3 desorbed from Brønsted acid sites.[17] The numbers of Brønsted acid sites calculated on the basis of the amount of NH_3 desorbed at approximately 250–550 °C are summarized in Table 1. A decrease in the number of Brønsted acid sites due to the decrease in the amount of framework Al atoms was observed. The acid strength can be discussed on the basis of the desorption temperatures, where the peaks associated with the desorption of NH_3 from Brønsted acid sites shifted to lower temperature with increasing Si/Al molar ratio, indicating a lower acid strength for the CHA(*X*)s compared with that for the SSZ-13. This difference in the acid strength likely originates from the positions of the Brønsted acid sites. FT-IR spectra of SSZ-13(10) and CHA(200) are shown in Fig. S6 (ESI†). The bands observed at 3660–3500 cm^{-1} are attributed to the O–H stretching vibration of the acidic OH groups.[17] Katada *et al.* reported that four types of O–H stretching vibrations occur in the **CHA**-type structure depending on the position of the acidic OH groups.[17] In the present study, the peak-top frequency for the acidic OH groups differs between SSZ-13(10) and CHA(200); the peak-top frequency for the main band of the acidic OH groups on SSZ-13(10) was 3612 cm^{-1}, whereas that for the acidic OH groups on CHA(200) was 3538 cm^{-1}. According to a previous report, the bands at 3612 and 3538 cm^{-1} are attributable to acidic OH groups in 6R and 8R zeolites, respectively, and the acid strength for the former species is weaker than that for the latter species.[17] This result is consistent with the NH_3-TPD results. That is, the proposed synthesis method can control the number of acid sites and their acid strength. In addition, the FT-IR spectra suggest the specific crystallinity of CHA(200). Although silanol nests are observed as broad bands at 3500–3300 cm^{-1} in the FT-IR spectra of conventional high-silica **CHA**-type zeolites,[18] they were not observed in the spectrum of CHA(200), indicating that the CHA(200) sample is highly crystalline. Such high crystallinity was also proved by ^{29}Si MAS NMR spectra (Fig. S7 and Table S3), where the peaks attributed to Q^3 species,[19] $Si(OSi)_3OH$, were observed at –101 ppm with extremely low intensity for all the samples.

Finally, the catalytic performance of the synthesized **CHA**-type aluminosilicates in the MTO reaction was evaluated. Fig. 2 shows the time courses of the catalytic activity over each sample at 350 °C. In the case of SSZ-13(10), the conversion dramatically decreased at ca. 5 h because of the large number of acid sites. The catalyst lifetime improved with increasing Si/Al molar ratio; CHA(50) exhibited the longest catalytic lifetime among the investigated catalysts, suggesting that an excessive reduction of the number of acid sites adversely affects the catalyst lifetime for the **CHA**-type zeolites. The dual-cycle hydrocarbon-pool mechanism has been proposed for the MTO reaction over cage-type zeolites.[1b,20] According to this mechanism, aromatic-based compounds are regarded as reaction intermediates that cannot pass through the pores of an 8R zeolite. Decreasing the number of acid sites to ca. 0.2 per *cha* cage (Table 1) is sufficient to suppress consecutive reactions. Therefore, an excessive reduction of the amount of acid sites might be an ineffective approach to improving the catalyst lifetime, rather causing a lack of catalytically active sites for the MTO reaction. Reducing the number of acid sites improved not

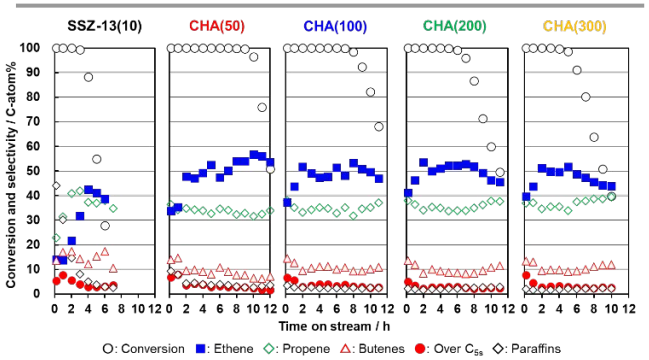

Fig. 2 Time courses of the MTO reaction at 350 °C over SSZ-13 and high-silica **CHA**-type aluminosilicates. Reaction conditions: 100 mg catalyst, 5 vol% methanol in Ar gas, W/F_{MeOH} = 68 g h mol^{-1}.

only the catalyst lifetime but also the selectivity toward lower olefins from the beginning of the reaction. The catalytic performance of the samples at 10 min of time on stream (TOS) is summarized in Table S2 (ESI†). In general, a large amount of paraffins was generated at the initial stage because of the high density of acid sites and high acid strength in the **CHA**-type aluminosilicates.[7b,21] Indeed, for SSZ-13(10), the selectivity toward paraffins reached 43%, whereas the total selectivity toward the lower olefins ($C_{2=}$ + $C_{3=}$ + $C_{4=}$) was as low as 51%. By contrast, the selectivity toward ethene and propene was improved by increasing the Si/Al molar ratio; this improvement originates from the suppression of the consecutive reaction to paraffins. Moreover, the selectivity toward ethene was further increased over CHA(200) and CHA(300). Between them, CHA(200) achieved the highest total selectivity toward lower olefins (93%). This selectivity is the most important benefit induced by the extremely high-silica **CHA**-type aluminosilicates.

In conclusion, extremely high-silica **CHA**-type aluminosilicates (Si/Al molar ratio > 100) with good crystallinity were successfully synthesized using seed-assisted aging treatment in the absence of fluoride media, where the highest Si/Al ratio achieved was 156. The fluoride-free conditions resulted in relatively small particles. In addition, the decrease in the number of framework Al atoms led to a decrease in not only the number of acid sites but also the acid strength. In addition, the synthesized high-silica **CHA**-type aluminosilicates exhibited excellent catalytic performance in the MTO reaction. Compared with the conventional SSZ-13 zeolite, the **CHA**-type aluminosilicates showed a longer catalyst lifetime and a greater selectivity toward the lower olefins. The novel synthetic method for the extremely high-silica **CHA**-type aluminosilicates reported in the present work is expected to contribute to upgrading the industrial chemical processes.

This work was financially supported by Core Research for Evolutional Science and Technology of the Japan Science and Technology Agency (Grant No. JPMJCR16P3), a Grant-in-Aid for Scientific Research (S) (Grant No. JP21H05011), and a Grant-in-Aid for Early-Career Scientists (JP21K14449) from the Japan Society for the Promotion of Science.

References

1 (*a*) A. Corma, *Chem. Rev.*, 1995, **95**, 559–614; (*b*) U. Olsbye, S. Svelle, M. Bjrgen, P. Beato, T. V. W. Janssens, F. Joensen, S. Bordiga and K. P. Lillerud, *Angew. Chem. Int. Ed.*, 2012, **51**, 5810–5831; (*c*) M. Dusselier and M. E. Davis, *Chem. Rev.*, 2018, **118**, 5265–5329; (*d*) P. del Campo, C. Martínez and A. Corma, *Chem. Soc. Rev.*, 2021, **50**, 8511–8595; (e) M. Yabushita, R. Osuga and A. Muramatsu, *CrystEngComm*, 2021, **23**, 6226–6233.

2 (*a*) M. Miyamoto, Y. Fujioka and K. Yogo, *J. Mater. Chem.*, 2012, **22**, 20186–20189; (*b*) H. W. B. Teo, A. Chakraborty and B. Han, *Appl. Therm. Eng.*, 2017, **127**, 35–45; (*c*) M. Yabushita, Y. Imanishi, T. Xiao, R. Osuga, T. Nishitoba, S. Maki, K. Kanie, W. Cao, T. Yokoi and A. Muramatsu, *Chem. Commun.*, 2021, **57**, 13301–13304.

3 L. S. Dent and J. V. Smith, *Nature*, 1958, **181**, 1794–1796.

4 S. I. Zones, *US Pat.*, 1985, 4,544,538.

5 (*a*) L. Wu, V. Degirmenci, P. C. M. M. Magusin, N. J. H. G. M. Lousberg and E. J. M. Hensen, *J. Catal.*, 2013, **298**, 27–40; (*b*) Q. Zhu, J. N. Kondo, R. Ohnuma, Y. Kubota, M. Yamaguchi and T. Tatsumi, *Microporous Mesoporous Mater.*, 2008, **112**, 153–161; (*c*) X. Zhu, J. P. Hofmann, B. Mezari, N. Kosinov, L. Wu, Q. Qian, B. M. Weckhuysen, S. Asahina, J. Ruiz-Martínez and E. J. M. Hensen, *ACS Catal.*, 2016, **6**, 2163–2177; (*d*) Z. Li, M. T. Navarro, J. Martínez-Triguero, J. Yu and A. Corma, *Catal. Sci. Technol.*, 2016, **6**, 5856–5863.

6 (*a*) F. Bleken, M. Bjørgen, L. Palumbo, S. Bordiga, S. Svelle, K. P. Lillerud and U. Olsbye, *Top. Catal.*, 2009, **52**, 218–228; (*b*) R. Osuga, T. Yokoi, K. Doitomi, H. Hirao and J. N. Kondo, *J. Phys. Chem. C*, 2017, **121**, 25411–25420.

7 (*a*) L. Sommer, D. Mores, S. Svelle, M. Stöcker, B. M. Weckhuysen and U. Olsbye, *Microporous Mesoporous Mater.*, 2010, **132**, 384–394; (*b*) T. Nishitoba, N. Yoshida, J. N. Kondo and T. Yokoi, *Ind. Eng. Chem. Res.*, 2018, **57**, 3914–3922.

8 (*a*) M. J. Díaz-Cabañas, P. A. Barrett and M. A. Camblor, *Chem. Commun.*, 1998, 1881–1882; (*b*) M. Miyamoto, T. Nakatani, Y. Fujioka and K. Yogo, *Microporous Mesoporous Mater.*, 2015, **206**, 67–74; (*c*) H. Al Jabri, K. Miyake, K. Ono, M. Nakai, Y. Hirota, Y. Uchida, M. Miyamoto and N. Nishiyama, *Microporous Mesoporous Mater.*, 2019, **278**, 322–326; (*d*) J. Zhang, P. Ji, L. Ren, Y. Zhao, S. Li, H. Xu, H. Peng, J. G. Jiang, Y. Guan and P. Wu, *Chem. Eng. J.*, 2022, **444**, 136657; (*e*) X. Kong, H. Qiu, Y. Zhang, X. Tang, D. Meng, S. Yang, W. Guo, N. Xu, L. Kong, Y. Zhang and Z. Zhang, *Microporous Mesoporous Mater.*, 2021, **316**, 110914; (*f*) X. Kong, H. Qiu, D. Meng, X. Tang, S. Yang, W. Guo, Y. Zhang, L. Kong, Y. Zhang and Z. Zhang, *Sep. Purif. Technol.*, 2021, **274**, 119104; (*g*) Y. Kubota, S. Inagaki and T. Fukuoka, JP Pat., P2016-169118A, 2016; (*h*) J. Zhou, F. Gao, K. Sun, X. Jin, Y. Zhang, B. Liu and R. Zhou, *Energy Fuels*, 2020, **34**, 11307–11314.

9 (*a*) S. I. Zones, R. J. Darton, R. Morris and S. J. Hwang, *J. Phys. Chem. B*, 2005, **109**, 652–661; (*b*) E. A. Eilertsen, B. Arstad, S. Svelle and K. P. Lillerud, *Microporous Mesoporous Mater.*, 2012, **153**, 94–99.

10 (*a*) H. Mochizuki, T. Yokoi, H. Imai, R. Watanabe, S. Namba, J. N. Kondo and T. Tatsumi, *Microporous Mesoporous Mater.*, 2011, **145**, 165–171; (*b*) D. Chen, K. Moljord, T. Fuglerud and A. Holmen, *Microporous Mesoporous Mater.*, 1999, **29**, 191–203; (*c*) Z. Xu, J. Li, Y. Huang, H. Ma, W. Qian, H. Zhang and W. Ying, *Catal. Sci. Technol.*, 2019, **9**, 2888–2897.

11 (*a*) K. Iyoki, K. Itabashi and T. Okubo, *Microporous Mesoporous Mater.*, 2014, **189**, 22–30; (*b*) N. Tsunoji, D. Shimono, K. Tsuchiya, M. Sadakane and T. Sano, *Chem. Mater.*, 2020, **32**, 60–74.

12 R. Osuga, T. Yokoi and J. N. Kondo, *J. Catal.*, 2019, **371**, 291–297.

13 (*a*) S. A. Pelster, W. Schrader and F. Schüth, *J. Am. Chem. Soc.*, 2006, **128**, 4310–4317; (*b*) B. B. Schaack, W. Schrader and F. Schüth, *Angew. Chem. Int. Ed.*, 2008, **47**, 9092–9095.

14 N. Martín, M. Moliner and A. Corma, *Chem. Commun.*, 2015, **51**, 9965–9968.

15 T. Moteki and R. F. Lobo, *Chem. Mater.*, 2016, **28**, 638–649.

16 M. Haouas, F. Taulelle and C. Martineau, *Prog. Nucl. Magn. Reson. Spectrosc.*, 2016, **94–95**, 11–36.

17 K. Suzuki, G. Sastre, N. Katada and M. Niwa, *Phys. Chem. Chem. Phys.*, 2007, **9**, 5980–5987.

18 M. Itakura, I. Goto, A. Takahashi, T. Fujitani, Y. Ide, M. Sadakane and T. Sano, *Microporous Mesoporous Mater.*, 2011, **144**, 91–96.

19 B. Fan, D. Zhu, L. Wang, S. Xu, Y. Wei and Z. Liu, Inorg. Chem. Front., 2022, 9, 3609–3618.

20 M. Fečík, P. N. Plessow and F. Studt, *Catal. Sci. Technol.*, 2021, **11**, 3826–3833.

21 N. Tsunoji, R. Osuga, M. Yasumoto and T. Yokoi, *Appl. Catal. A Gen.*, 2021, **620**, 118176